communications earth & environment

Article

https://doi.org/10.1038/s43247-024-01317-7

A framework to assess permafrost thaw threat for land transportation infrastructure in northern Canada

Check for updates

Ali Fatolahzadeh Gheysari [1] & Pooneh Maghoul [1,2]

Prediction of permafrost stability is associated with challenges, such as data scarcity and climate uncertainties. Here we present a data-driven framework that predicts permafrost thaw threat based on present ground ice distributions and ground surface temperatures predicted via machine learning. The framework uses long short-term memory models, which account for the sequential nature of climate data, and predicts ground surface temperature based on several climate variables from reanalysis products and regional climate models. Permafrost thaw threat is then assessed for three cases in northern Canada: Hudson Bay Railway, Mackenzie Northern Railway, and Inuvik–Tuktoyaktuk Highway. The models predict ground surface warming in all studied areas under both moderate and extreme climate change scenarios. The results also suggest that all studied cases are already under threat, with the northern sections of the Hudson Bay Railway and Inuvik–Tuktoyaktuk Highway facing an increasing threat by the end of the century.

Despite having 0.1 percent of the world's population, the Arctic region currently generates about 0.7 percent of the global gross domestic product, mainly from oil production, mining, food, and tourism. Over the recent past decades, the Arctic region has experienced socioeconomic development, e.g., the region's share in global gross domestic product increased by 60 percent between 2005 and 2018[1,2]. The socioeconomic outlook of the Arctic is projected to change over the next few decades. The population in northern Canada and Alaska is projected to increase by 10% by 2055[3]. The loss of sea ice due to global warming has provided marine transportation opportunities in the Arctic and subarctic regions. It has been reported that the marine traffic in northern Canada, including shipping through the Northern Passage, commercial fishing, and marine tourism, has nearly tripled during the past 30 years. The transit times across the Northern Sea Route have been reduced, mainly attributed to global warming and the subsequent loss of sea ice[4,5].

On the other hand, the warming of the climate system is the major forcing in destabilizing permafrost, threatening communities and infrastructure in the Arctic and subarctic mainland and coastal areas. Permafrost, defined as the layer below the ground surface that remains at or below 0 °C for at least two consecutive years, covers more than 15% of the northern hemisphere and 50% of the land mass in the Arctic Circle. It also extends to the subarctic latitudes and exists in mountainous areas, mostly in the form of discontinuous or sporadic patches of permafrost[6–9]. Currently, the Arctic permafrost area hosts about 5 million inhabitants living in more than 1100 settlements[10]. About 44,000 km of roads, 7000 km of railway, 380 airports, and 9500 km of pipelines have been built on the Arctic permafrost[11].

Observations of the recent past climate reveal the warming in the Arctic region is higher than the global averages[12]. Between 2007 and 2016, the mean temperature of continuous and discontinuous permafrost at the depth of zero annual amplitude—the depth beneath which there is no annual temperature fluctuation—increased by 0.39 ± 0.15 °C and 0.20 ± 0.10 °C, respectively[13]. The sensitivity of permafrost to global warming, i.e., the area of permafrost thawed as a result of 1 °C global mean warming, is estimated at 4.0 million km^2 per °C[14]. The thawing of permafrost has potential adverse effects on global climate, ecosystems, communities, and infrastructure. From a geotechnical perspective, the warming of permafrost is associated with the loss of soil strength and results in ground deformations, ranging from slow-paced creep to rapid thaw settlements and landslides[15,16]. In ice-rich permafrost, the thawing is associated with a loss of soil volume in a brief period of time, resulting in thermokarsts[17]. In addition to the existing infrastructure, permafrost degradation also affects the design and planning of new infrastructure. For instance, in the case of land transportation infrastructure, the occurrence of thermokarsts, thaw slumps, and landslides

[1]Sustainable Infrastructure and Geomechanics Laboratory (SIGLab), Department of Civil Engineering, University of Manitoba, Winnipeg, MB, Canada. [2]Sustainable Infrastructure and Geomechanics Laboratory (SIGLab), Civil, Geological and Mining Engineering Department, Polytechnique Montréal, Montreal, QC, Canada. e-mail: pooneh.maghoul@polymtl.ca

may change or limit accessibility and hence require longer travel paths to avoid unstable areas[18].

Several studies assessed the regional impacts of permafrost degradation on communities and infrastructure. It is estimated that by 2050, permafrost will degrade in more than 500 communities, affecting 3.3 million residents[10]. By the mid-century, the majority of infrastructure on the Arctic permafrost will be subjected to permafrost thaw[11], which highlights the need for adaptation measures[19]. The development of regional ground ice and soil type distributions have facilitated the definition of vulnerability indices for permafrost[20,21]. Near-surface (ambient) air temperature is often used as a threat indicator for the thermal stability of permafrost due to the correlation between ground temperature and atmospheric conditions above the ground surface. Ambient temperature is one of the essential climate variables that are available in global and regional climate prediction models. However, the ground thermal regime is in fact, governed by the surface energy budget, thermal properties of the ground, and the presence of groundwater and ground ice[16]. Numerical simulations have been used to calculate the ground thermal regime. Nevertheless, the multi-physics simulation of the surface energy budget is challenging due to the multitude of physics involved, such as ambient temperature, solar radiation, convection through wind, and the effects of snow coverage and vegetation[22]. Ground surface temperature, another indicator for permafrost stability, is the resultant of the surface energy budget and has been used as the surface boundary condition in geotechnical and soil science numerical simulations to eliminate the inclusion of surface energy budget in models[23]. Ground surface temperature is not as readily available as ambient temperature since its measurement requires ground-mounted sensors and therefore, is often estimated from ambient temperature via conversion factors, known as n-factors[24]. The n-factors, however, neither reflect the effects of other components of the surface energy budget nor their dynamic correlation in regard to climate change. Moreover, climate prediction models often do not provide ground temperature projections due to limitations in land surface schemes and the complexity of the surface energy budget. Therefore, the prediction of a robust indicator of permafrost degradation for threat assessments at local or regional scales remains a challenge.

With the amount of collected data increasing exponentially, the data-driven approach, including machine learning (ML), is nowadays widely used to detect correlations, patterns, and trends. Several studies have been conducted to estimate or forecast short-term ground temperature via data-driven techniques, including artificial neural networks (ANN)[25], extreme learning machines (ELM), generalized regression neural networks (GRNN), backpropagation neural networks (BPNN), random forests (RF)[26], and autoregressive integrated moving average (ARIMA)[27]. However, these studies generally do not regard the sequential nature of the data, i.e., the correlation between climate variables in regard to time or address long-term climate change uncertainties. Recurrent neural networks (RNN), including long short-term memory (LSTM) and gated recurrent unit (GRU) networks, have recently been used to address temporal dynamics in time series data[28,29]. LSTM and GRU have been utilized in the short-term prediction of climate variables such as ground temperature and moisture, sea surface temperature, and solar irradiance[30–32]. It has been shown that past weather station records and projections from regional climate models can be used to forecast long-term ground surface temperature in the Arctic zone and lower latitudes[33]. However, the implementation of this approach in regional and subregional scales requires the input data to be available across the entire study area, which in the case of ground temperatures measured from boreholes, cover a small fraction of the Arctic and subarctic regions[34].

The spatiotemporal scarcity of climate measurements has been addressed by data assimilation and reanalysis models[35,36]. The reanalysis process can synthesize data for decades back in time, which can demonstrate the past changes in the climate system[35]. Among numerous reanalysis products, the Modern-Era Retrospective Analysis for Research and Applications (MERRA2) and the European Reanalysis (ERA) family have been used in a wide range of applications[37,38]. Studies on the Arctic, North America, and Europe have reported improved performance of ERA5 in comparison to MERRA2 and other global reanalysis products[39,40]. ERA5-Land, the land component of ERA5 for land surface applications, provides land surface climate data from 1950 to the present at a spatial resolution of 0.1° x 0.1° (~9 km)[41]. The ERA5-Land estimates have been previously evaluated in the circumpolar permafrost and the lower latitudes[42–44]. They reported an overestimation of ground temperatures, i.e., warm bias, in circumpolar permafrost in Alaska and Western Canada, and an underestimation in Qinghai–Tibetan Plateau's mountain permafrost, resulting in an average bias of –0.08 °C[42]. Reanalysis products have been used for training machine learning models for short-term climate forecasting due to their potential in addressing temporal and spatial scarcity of climate variables[45–47].

This study aims to address several challenges in permafrost thaw threat assessments, including the spatiotemporal scarcity of ground temperature data, the multivariate correlation between ground temperature and ambient climate variables, and the infeasibility of high-resolution multi-physics numerical simulations in regional scales. In this regard, a framework was developed to assess permafrost thaw threat by predicting long-term ground surface temperatures using reanalysis data (ERA5-Land) and regional climate projections (CanRCM). The framework calculates a thaw index, based on the projections of ground surface temperature and the present distribution of ground ice, which provides a rapid assessment of permafrost thaw threat at regional and subregional scale. Furthermore, the performance of the framework is evaluated, and thaw indices for permafrost degradation are presented for three major land transportation infrastructure in northern Canada: Hudson Bay Railway, Mackenzie Northern Railway, and the Inuvik–Tuktoyaktuk Highway.

Study cases

Hudson Bay Railway

The Hudson Bay Railway, known by the reporting mark HBRY, is a 1300 km railway extending between Flin Flon on the Manitoba-Saskatchewan border and the port of Churchill in northwest Manitoba (Fig. 1). It was also the name of the historic railway between Winnipeg and Churchill that was completed by the early 1930s. The railway brings freight and passenger train access to several communities in northern Manitoba and is the sole land link to Churchill. Churchill is a strategic port that provides access to the Northwest Passage, also known as the polar bear capital of the world, which is a major tourist attraction in the province.

Crossing the permafrost front, there is a northward transition from sporadic permafrost near Thompson, to extensive discontinuous permafrost, and continuous permafrost from M'Clintock to Churchill. During the railway's operation history, settlements had occurred along embankments in many locations, which required backfilling with large amounts of granular fill. Settlements as much as 100–150 mm due to the thawing of ice-rich permafrost have been reported[48]. Ground ice exists in the form of segregated ice in the area, according to the ground ice map of Canada[20]. The section between Gillam to Herchmer, which lies on extensive discontinuous permafrost, has been reported to be the most problematic in terms of flooding and thaw settlements[49,50]. In this study, the 400 km section between Thompson and Churchill was chosen as a study area.

Mackenzie Northern Railway

The Mackenzie Northern Railway, identified by the reporting mark RLGN, is a 969 km long railway that runs from Grimshaw in Alberta to Hay River in the Northwest Territories. Construction of the railway began in 1961 and was completed in 1964. The Mackenzie Northern Railway is the only railway in Canada that intersects the 60th parallel. Hay River, which serves as a hub for rail, river, and road transportation, marks the northernmost point of the contiguous North American railway network. The railway plays a critical role in the transportation of land freight to the Northwest Territories, with around 50 percent of all freight being carried by it, making it an essential lifeline for the communities and mining industry in the region.

The railway traverses the permafrost front, transitioning from sporadic permafrost southward to discontinuous permafrost extending between

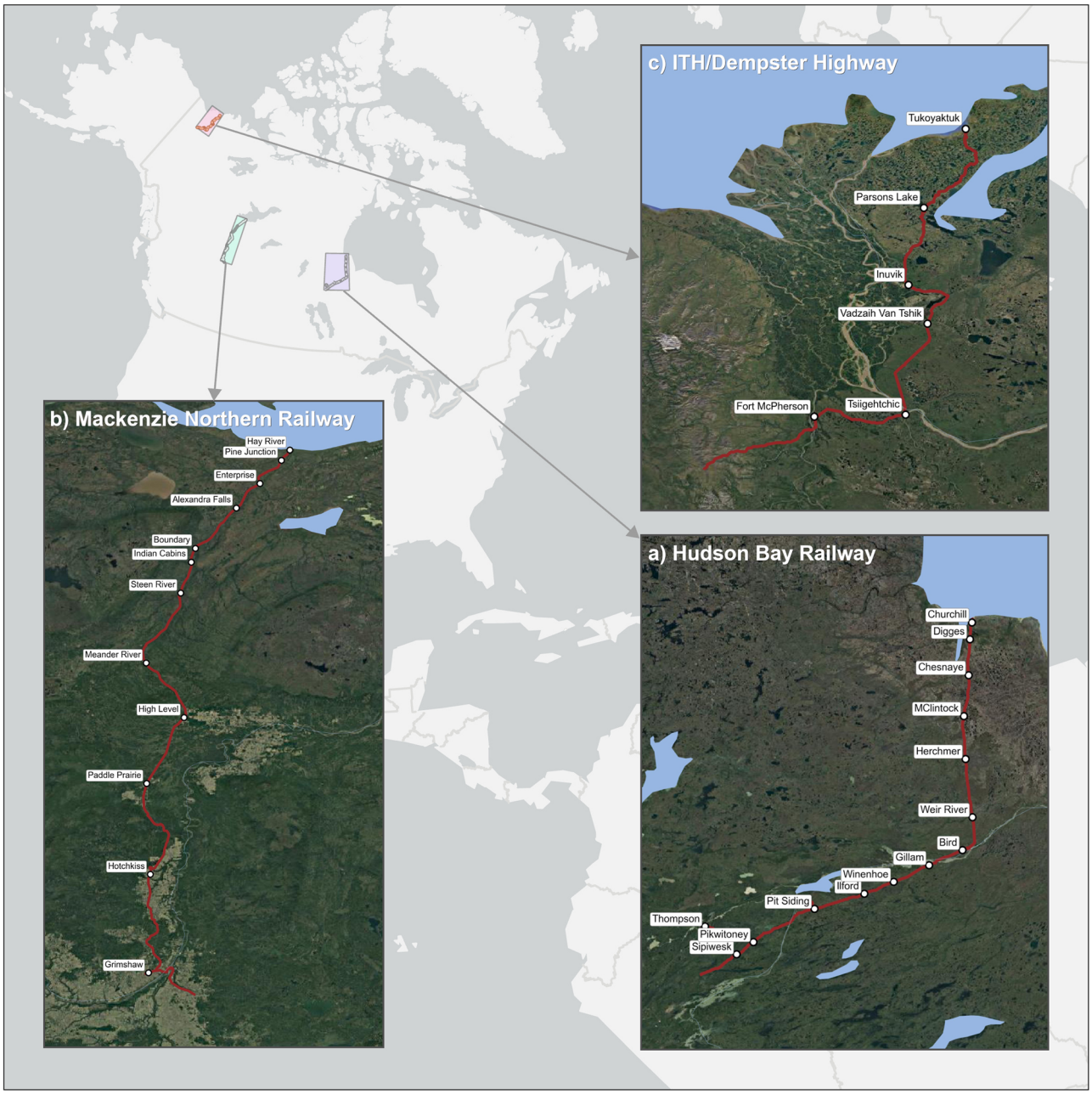

Fig. 1 | Location of case studies. a Hudson Bay Railway. **b** Mackenzie Northern Railway. **c** Inuvik–Tuktoyaktuk/Dempster Highway. Satellite imagery: Google, Landsat/Copernicus, IBCAO. Map sources: Esri, HERE, Garmin, FAO, NOAA, USGS, ©OpenStreetMap contributors, and the GIS User Community.

High Level and the Alberta-Northwest Territories boundary. Ground ice exists in the form of segregated ice. Although there are no reports of direct damage to the railway due to permafrost thawing in the literature, the railway operates with a limited restriction of 220,000 lbs, which is lower than the national standard of 286,000 lbs. For the purpose of this study, the 969 km section of the railway between Grimshaw and Hay River was chosen for calculating permafrost thaw indices.

Inuvik–Tuktoyaktuk Highway and Dempster Highway

The Inuvik–Tuktoyaktuk Highway, also known as Northwest Territories Highway 10, is an all-weather road spanning 138 km between Inuvik and Tuktoyaktuk in Mackenzie Delta in the Northwest Territories. The highway opened to the public in 2017, following the start of construction in 2014. The road is built on both discontinuous and continuous permafrost, with abundant ground ice present in the form of segregated, relict (buried glacier), and wedge ice. The area has experienced abrupt changes in permafrost due to climate warming, as well as thawing caused by construction activities. These changes have resulted in settlements, embankment instability, and retrogressive thaw slumps[51]. This study assesses a 324 km section of the highway, including the Inuvik–Tuktoyaktuk Highway and a 186 km section of the Dempster Highway within the Northwest Territories, between Fort McPherson and Inuvik.

Results

Validation and errors

A blind validation scheme is taken to validate the predictions and evaluate the model performance by comparing the predicted ground surface temperatures versus ERA5-Land counterparts over a test period excluded from the training data. Here, the ERA5-Land data serves as the actual data since it has been used for model training and validation. The predicted and actual daily ground surface temperatures at selected points of interest and the predicted and actual mean annual ground surface temperatures at all grid

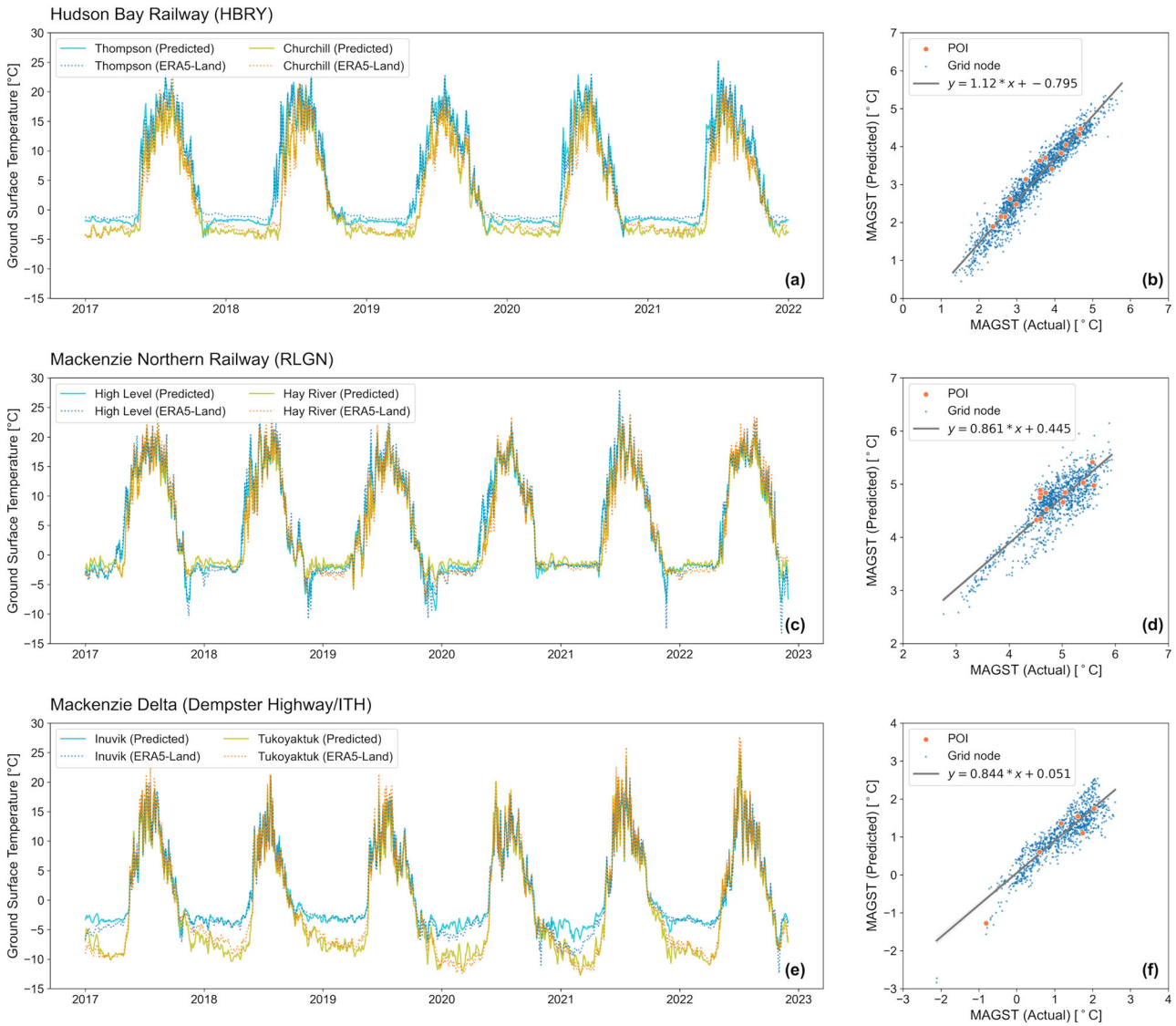

Fig. 2 | Validation of model predictions. a–c Comparison of daily predicted and actual (ERA5-Land) ground surface temperatures over the test period. **d–f** Comparison of predicted and actual MAGST at grid nodes and points of interest over the test period.

nodes are presented for a test period between 2017 and 2023 for each study area, as shown in Fig. 2. The models' ability to predict ground surface temperature over the test period was evaluated using various statistical metrics, including bias, mean absolute error (MAE), root mean square error (RMSE), and maximum absolute error (MaAE) at each node. The summary of errors, which includes the mean and maximum spatial bias, MAE, MaAE, and RMSE, is presented in Table 1. The errors at each grid node are presented in Supplementary Data 1.

It should be noted that the validation of the models was not conducted on the projection dataset due to the lack of the dependent variable in the projection dataset (CanRCM) and the fact that even in the presence of a labeled projection set, treating climate models' predictions as "actual" would not result in a meaningful evaluation, considering their inherent uncertainties. Therefore, only the test dataset was used for the purpose of validation.

The ground ice indices used in the forecasting framework were derived from the Ground Ice Map of Canada (GIMC), in which the ground ice abundance has been evaluated and found to be consistent with observations at several study sites, including Mackenzie Delta and Hudson Bay lowlands. For more information on the evaluation approach for ground ice content, the reader is referred to the Ground Ice Map of Canada's publication[20].

Ground surface temperature and thaw index projections

The CanRCM projection datasets were used to model ground surface temperatures under RCP 4.5 and RCP 8.5 scenarios until the year 2100. Mean annual temperatures were then calculated and compared at two specific instances: mid-century and end of the century. However, to account for the interannual variability of the climate, the decadal averages of

Table 1 | A summary of ground surface temperature prediction errors, including the spatial mean and maximum for each study region

	MBE		MAE		MaAE		RMSE	
	μ [°C]	max [°C]	μ [°C]	max [°C]	μ [°C]	max [°C]	μ [°C]	max [°C]
Hudson Bay Railway	0.38	1.40	0.44	1.40	0.72	1.96	0.28	2.05
Mackenzie Northern Railway	0.23	1.05	0.34	1.05	0.65	1.58	0.19	1.20
Inuvik–Tuktoyaktuk Highway	0.13	1.33	0.39	1.33	0.80	2.03	0.24	1.94

The errors are calculated as temporal averages over the test period. The temporal errors at each node are presented in the Supplementary Data 1 in detail.

1950–1960, 2010–2020, 2040–2050, and 2090–2100 were selected to represent the past, present, mid-century and late-century milestones. The plots of mean annual ground surface temperature (MAGST) (Fig. 3) reveal a notable variation in temperature across the examined regions and demonstrate the warming of the ground surface with respect to climate change.

Using these ground surface temperature projections, the distribution of the thaw index is calculated across the study areas for the present time, mid-century, and by the year 2100 under both moderate and extreme climate change scenarios (Fig. 4 and Supplementary Data 2–3). The plots indicate a spatial variation in the thaw index within and between the studied regions following ground surface warming and the existing ground ice. Notably, the discontinuous spatial variation of the thaw index within study areas largely follows ground ice content, as MAGST (as shown in Fig. 3) is relatively uniform across the study regions.

For a quantitative presentation of ground surface warming due to climate change and the subsequent threat to permafrost, MAGST anomalies and the thaw indices are plotted versus time at the major points of interest (Fig. 5 and Supplementary Data 4). The results reveal that by the end of the century, MAGST at the major points of interest will increase by 1.03–2.90 °C and 3.48–4.82 °C under RCP 4.5 and RCP 8.5 scenarios, respectively (Fig. 5a, b). The models also indicate higher warming at the Mackenzie Delta (Inuvik–Tuktoyaktuk Highway and Dempster Highway) site, which may be attributed to the Arctic amplification phenomenon[52].

According to the thaw index distributions (Fig. 4), the thaw index gradually increases northeastward in the Hudson Bay Railway study area, which is generally aligned with the ice content distribution. A minor increase in thaw index versus time has been observed at Churchill and Herschmer stations (Fig. 5c, d). Also, by plotting the thaw index at points of interest along the studied infrastructure (Fig. 6), it is possible to speculate that the abrupt rise in thaw index between the Herchmer and M'Clintock could indicate the boundary between affected and unstable permafrost. This supposition is based on two observations. Firstly, the thaw index in the south of Herchmer appears to be relatively unaffected by time and climate change scenarios (Fig. 4), which could suggest that thawing has already begun in this region. Additionally, previous reports have indicated that the majority of settlements occurred between Gillam and Herchmer[49,50], which implies that the thaw front is shifting towards the northeast.

In the Mackenzie Northern Railway study site, the thaw index remains unchanged despite the projected warming in the area due to climate change (Fig. 4). South of Paddle Prairie, the thaw index is nil due to the absence of excess ground ice and then increases northward, where the discontinuous path of permafrost exists, before decreasing toward the Hay River. As already speculated above, no changes in the thaw index between the present time and the future at this site would imply that the thawing has already begun, which can be supported by relatively higher ground surface temperatures than the other study areas.

Of all the study regions, the Mackenzie Delta area, including the Inuvik–Tuktoyaktuk Highway and Dempster Highway, exhibited the highest levels of thaw indices (Fig. 4). Also, contrary to the other study regions, the thaw indices will noticeably change over time and with respect to climate change. For instance, in Tuktoyaktuk, the thaw index will increase from approximately 0.15 in 2010–2020 to 0.34 and 0.62 in 2090–2100, under RCP 4.5 and RCP 8.5, respectively (Fig. 5c, d). It is noteworthy that the thaw index was found to be nil at the exact location of the Fort McPherson hamlet (Fig. 6) due to the absence of excess ground ice, according to the Ground Ice Map of Canada. However, the distribution of the thaw index (Fig. 4) indicates abrupt changes in the vicinity of Fort McPherson due to the abrupt changes in the ground ice content. It should also be noted that the jaggedness of the distribution map along the Arctic coastline is due to the difference between coastline boundaries in ERA5-Land and CanRCM, which causes inconsistent model inputs and results in null predictions by the model.

Discussion

It is important to note that the developed thaw indices present the risk in comparison to the present conditions. In other words, the thaw index at a given point in time (t) estimates the overall risk of instability that may occur by (t), relative to present conditions. This approach might provide a better correlation with risk assessment practices, as stakeholders often seek to understand the threats posed to infrastructure during its design life.

Monitoring the thaw index changes over time and at multiple instances in the future can provide insights into the periods in which thawing threats are more likely to occur. Also, it can help determine whether the infrastructure is already at risk, or if the impacts are expected in the future. A summary of possible cases for thaw index and their interpretation is presented in Table 2. The predictions of MAGST suggest warming of the ground surface by the end of the century, with an average of 2.1 °C and 4.1 °C at studied sites under the RCP 4.5 and RCP 8.5 scenarios, respectively. However, the thaw index depends on whether the present and projected ground temperatures are above or below the freezing point. An above-zero MAGST at present implies that permafrost, if present, is already subject to thaw. Among the areas of study, the Mackenzie Northern Railway area and the southern section of the Hudson Bay Railway area are examples of this condition. It should be noted that the abundance of ground ice also governs the magnitude of the threat. The thaw index is nil, i.e., interpreted as no significant risk, when no ground ice is present at the site. However, this interpretation is only valid within the definition of ground ice indices and should not be used to draw conclusions about any unaccounted type or depth of ground ice, such as seasonal ground ice within the active layer. On the other hand, an increase in thaw index versus time implies that MAGST is currently below or at freezing temperature but will warm up well above freezing point, posing a further threat in the future. Yet, based on the definition of the thaw index, the magnitude of the threat depends on the ground ice abundance at the site. An example of this pattern was observed across the Mackenzie Delta and the northeast part of the Hudson Bay Railway area.

The range of errors in ground temperature predictions, with a mean RMSE of less than 0.3 °C and MaAE of less than 2 °C, indicates an accuracy that makes the results suitable for many applications. For studies at the regional and subregional scales, the proposed thaw index provides a rapid assessment of permafrost thaw threat by including both elements of climate warming and the presence of ground ice, which are not currently addressed by the traditional practice, such as the n-factors method. Scalability is another advantage of the proposed approach. Once the machine learning models are trained for a study area, various projection datasets, i.e., independent variables from different climate models or under various climate change scenarios, can be used to predict a range or ensemble of thaw threats without needing the models to be re-trained.

The proposed approach also has potential in local or engineering-scale threat assessments. The complexity of the surface energy budget in thermal and thermo-hydro-mechanical simulations can be reduced by using the framework's long-term predictions of ground surface temperature as boundary conditions, facilitating detailed simulation of permafrost stability under the infrastructure subject to climate nonstationarity. The AI-based long-term predictions of ground surface temperature address the shortcomings of the traditional n-factors method by the inclusion of climate nonstationarity and the multivariate nature of the surface energy budget. In this study, ambient temperature, solar radiation, wind speed, and snow depth were used as model features. If available, additional independent variables with high spatial variation, e.g., snow density and vegetation, can be included as training features, to improve model predictions locally. However, it is crucial to ensure such features are present in both the training and projection datasets used in the framework. Moreover, the proposed thaw index formulation can be refined to address local elements with high spatial variation. Some examples of such data are subsurface conditions, permafrost depth, drainage, and the presence of taliks. Furthermore, digital elevation models and soil information datasets, e.g., SoilGrids[53], can provide additional information, including ground surface slope and thermal

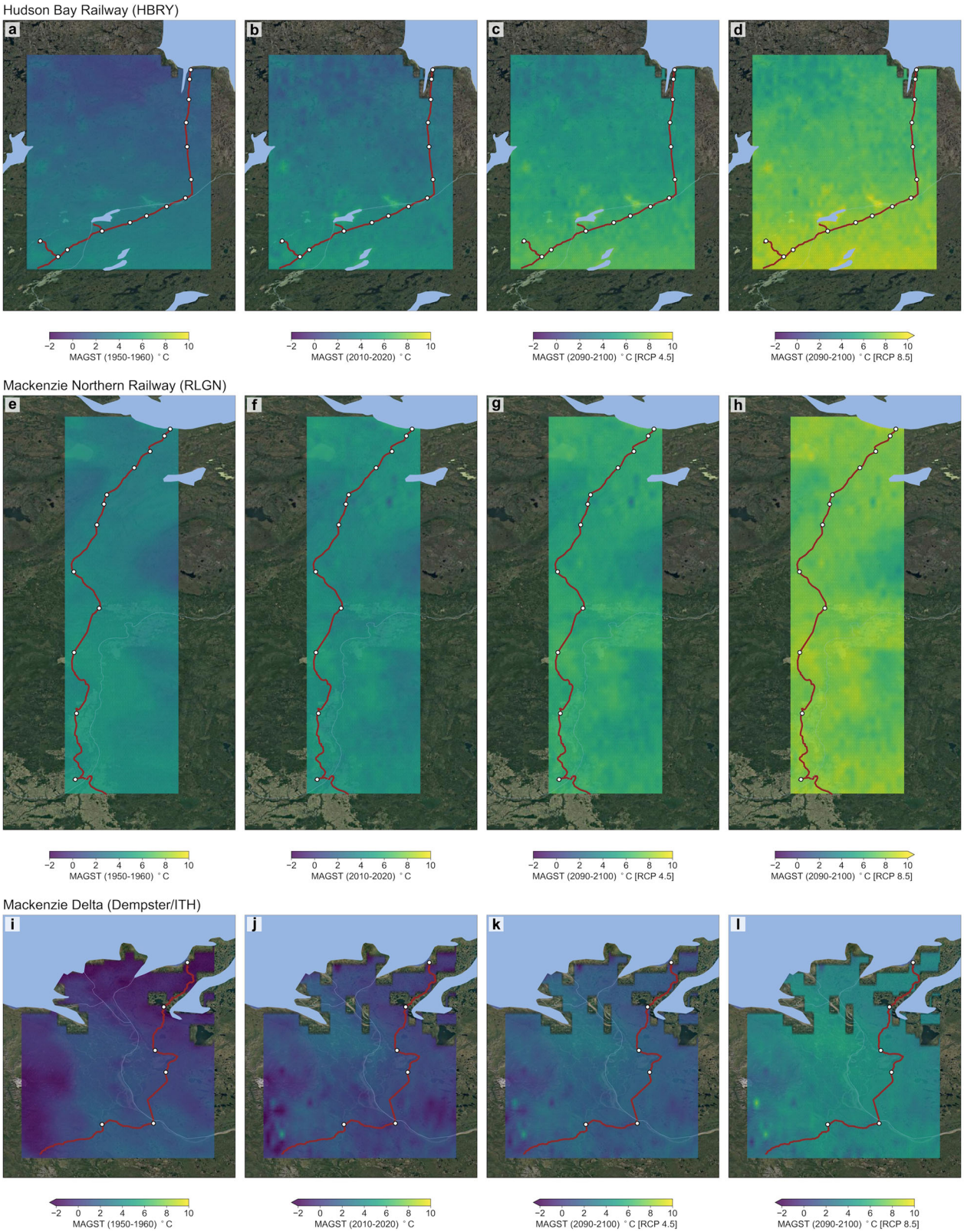

Fig. 3 | Distribution of past, present, and projected mean ground surface temperatures. a–d Hudson Bay Railway. **e–h** Mackenzie Northern Railway. **i–l** Inuvik–Tuktoyaktuk/Dempster Highway. **a**, **e**, **i** ERA5-Land 1950–1960 mean. **b**, **f**, **j** CanRCM 2010–2020 mean. **c**, **g**, **k** 2090–2100 predicted mean under RCP 4.5. **d**, **h**, **l** 2090–2100 predicted mean under RCP 8.5. Background satellite imagery: Google, Landsat/Copernicus, IBCAO.

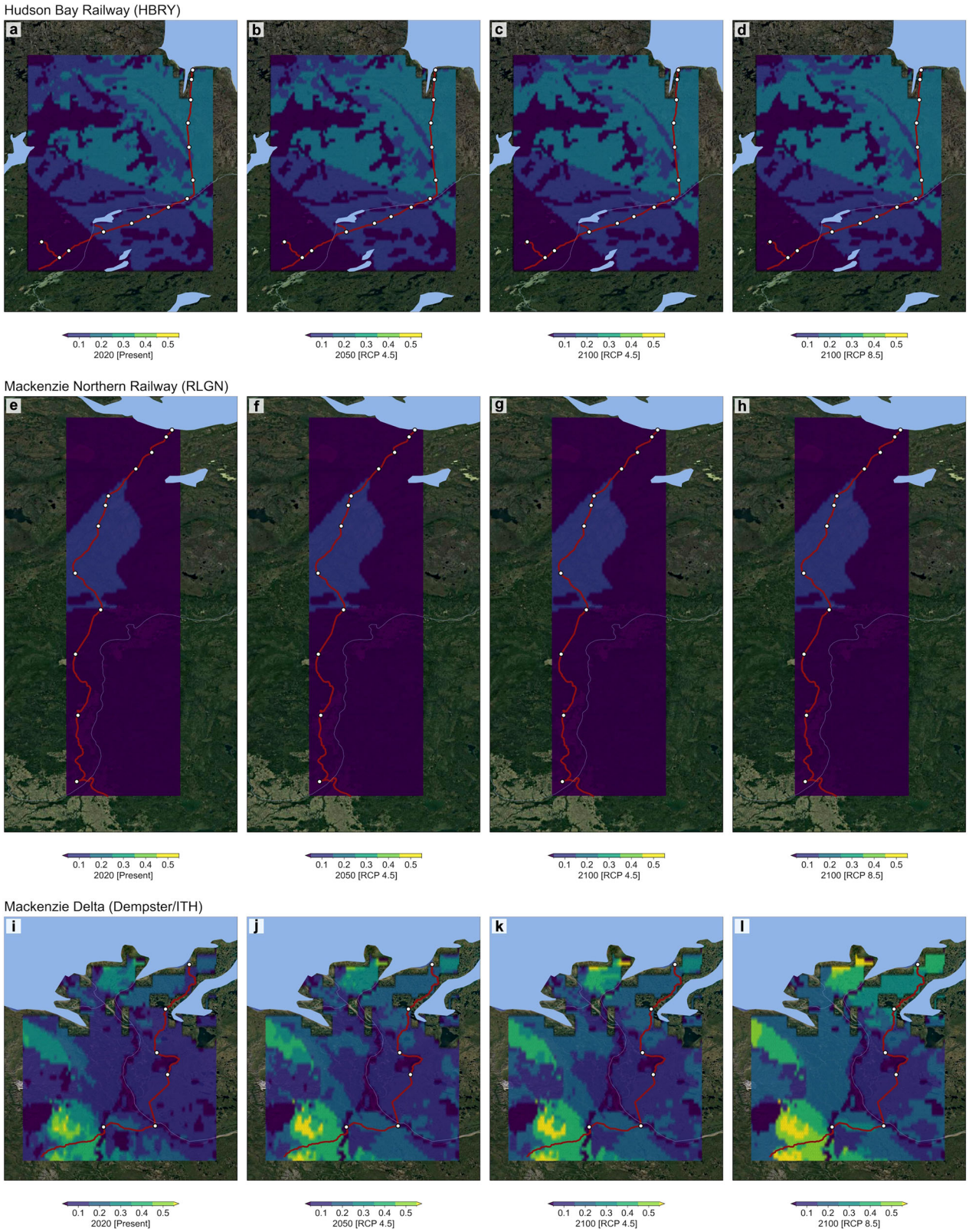

Fig. 4 | The present and projected distribution of permafrost thaw index. **a**–**d** Hudson Bay Railway. **e**–**h** Mackenzie Northern Railway. **i**–**l** Inuvik–Tuktoyaktuk/Dempster Highway. **a**, **e**, **i** Present (2020) estimate. **b**, **f**, **j** Prediction by 2050 prediction under RCP 4.5. **c**, **g**, **k** Prediction by 2100 under RCP 4.5. **d**, **h**, **l** Prediction by 2100 under RCP 8.5. Background satellite imagery: Google, Landsat/Copernicus, IBCAO.

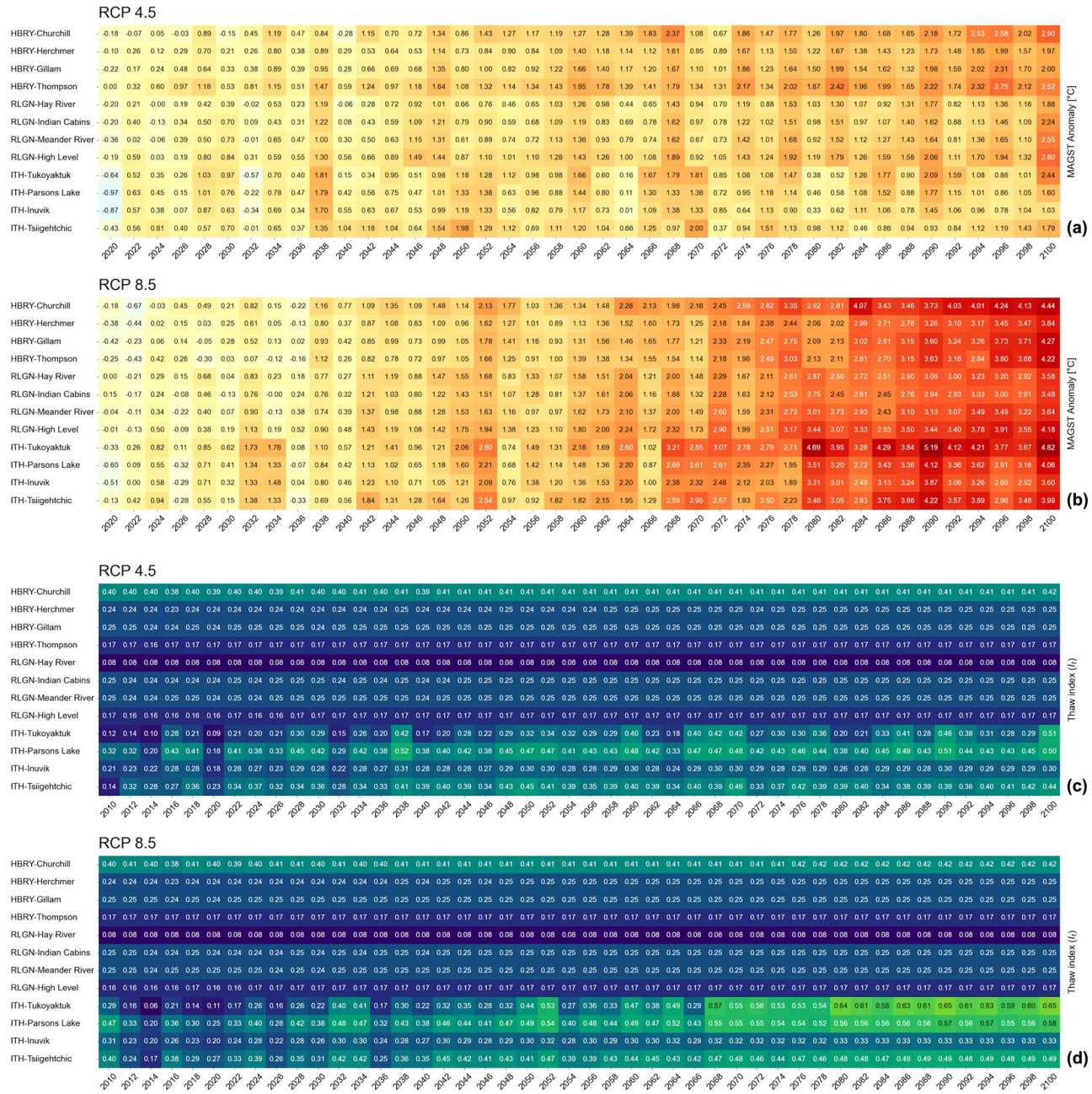

Fig. 5 | Projections of mean annual ground surface temperature anomalies and permafrost thaw index. a, **b** Mean annual ground surface temperature anomalies (2010–2020 baseline). **c**, **d** permafrost. The projections by 2100 under RCP 4.5 and RCP 8.5 climate change scenarios are presented for points of interest. The projections have been aggregated and presented as biennial means to improve readability.

properties of soil, which can further improve model performance, especially in local-scale threat assessments.

It should be noted that this paper aimed to demonstrate an overview and potential of the proposed AI-based framework. Here, equal weight factors were assumed for different types of ground ice. However, different types of ice can pose varying degrees of hazards to infrastructure in cold regions. For example, retrogressive thaw slumps are more common in relict ice, while the thawing and formation of segregated ice lenses are associated with frost heaving and thaw settlement[54,55]. Hence, weight factors could be adjusted to define thaw indices that represent specific threats to the infrastructure, depending on the subject and scope of the threat assessments.

The data-driven approach implies that the performance of the framework in predicting the thaw index would be heavily dependent on the training and projection data. In other words, the predictions inherit the uncertainties in training and projection datasets, in this study, ERA5-Land, CanRCM, and GIMC. These datasets were selected due to their spatial continuity to obtain spatial distributions of the thaw index. In the presence of training data with less uncertainty, such as direct measurement of climate variables from weather stations at points of interest, the framework could predict the local thaw index with reduced uncertainty. Moreover, this study used classic LSTM models to predict ground surface temperatures, which resulted in prediction errors on par with uncertainties in the ERA5-Land training data. Yet machine learning is an area of rapid evolution, and therefore, the framework could benefit from more advanced machine learning methods for sequential data, subject to further evaluation. Additionally, to address the uncertainties in projected independent variables, an ensemble of climate projections could be used, which would result in an

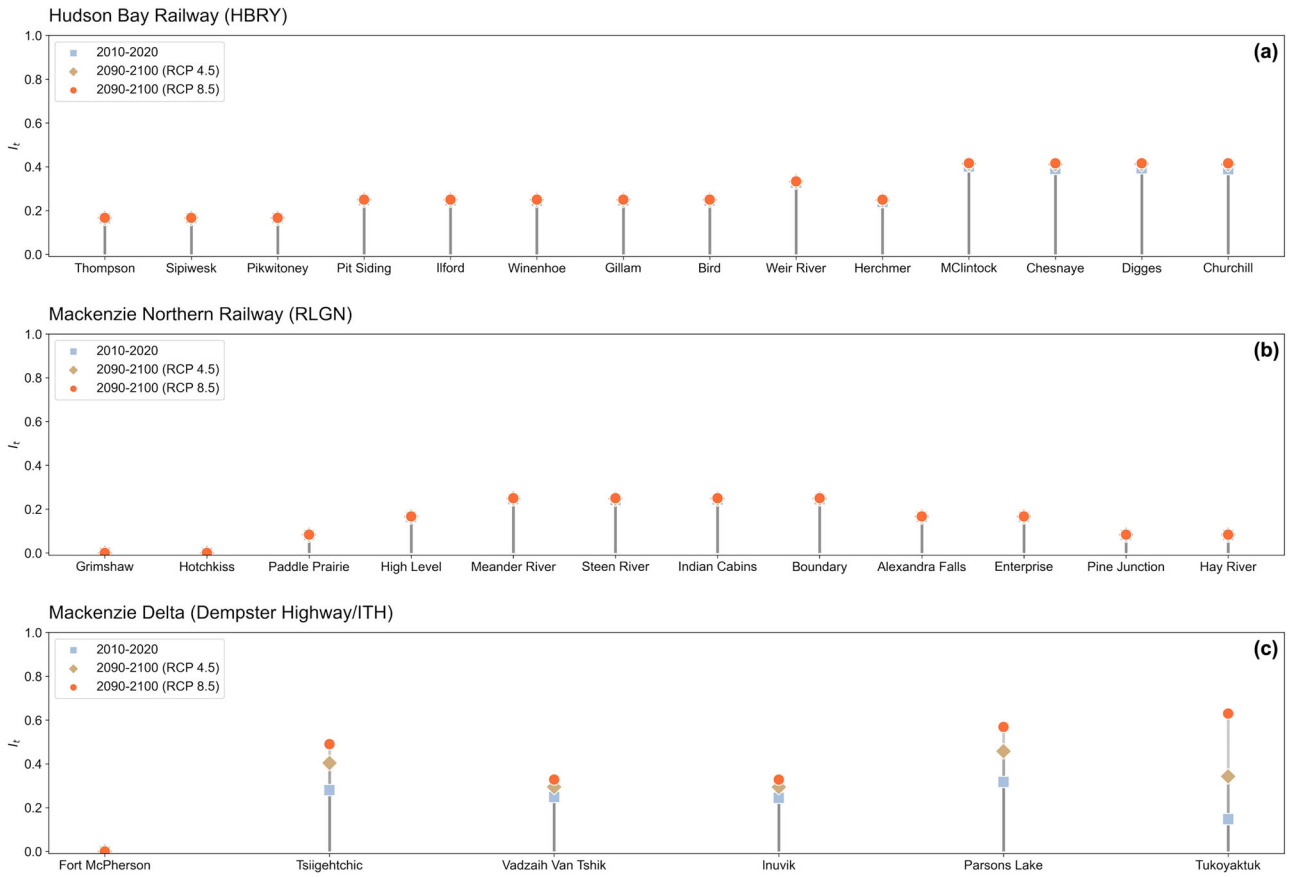

Fig. 6 | Present and predicted permafrost thaw index along the studied infrastructure. a Hudson Bay Railway. **b** Mackenzie Northern Railway. **c** Inuvik–Tuktoyaktuk/Dempster Highway. Note: the horizontal distances between the data points on the plot do not reflect the actual distance between the points of interest.

ensemble of GST and ice content based on various climate models and scenarios.

Conclusion

In conclusion, the developed threat assessment framework can address several challenges in the assessment of permafrost thawing threats, including the spatiotemporal scarcity of ground temperature data, complexity of surface energy budget, and the lack of tools for rapid assessment of permafrost thaw at the regional and subregional scales.

Using a data-driven approach assisted by machine learning techniques tailored for sequential data, the framework takes into consideration multiple elements of the surface energy budget as well as the dynamic nature of the climate system. The evaluation of the machine learning models indicated a consistency between the predictions and test data. The accuracy of predictions can be further enhanced in the presence of more robust training data or with the addition of information layers due to the modular structure of the framework.

Table 2 | Interpretation of thaw threat based on the present and predicted thaw index

$I_t^{t_0[present]}$	$I_t^{t_i[future]}$	Threat Interpretation
Low	Low	If $I_s, I_w, I_r \approx 0$: No significant threat at $t_0 \le t \le t_i$, [no ground ice]
		If $I_s, I_w, I_r \ge 0$: No significant threat at $t_0 \le t \le t_i$, $[f(MAGST)_{t_0,t_i} \approx 0]$
Low	High	Stable at t_0, but will be under threat by t_i, $[f(MAGST)_{t_0} \approx 0, f(MAGST)_{t_i} > 0]$
High	High	Currently under thaw threat

The studied cases reveal the dynamic nature of thawing threats, including temporal and spatial variety. All studied regions demonstrated thawing threats. The northern section of the Hudson Bay Railway and the majority of the Mackenzie Delta region will experience shifting thawing fronts and an increased risk of thawing due to ongoing global warming in the near future. Meanwhile, the other studied regions have already experienced or are currently facing instabilities due to thawing.

Based on the results, the proposed thaw threat assessment framework can be useful in a wide range of applications, including but not limited to engineering design, infrastructure asset management, and environmental stewardship. By providing a more comprehensive understanding of the potential threats associated with permafrost thaw, stakeholders can better assess, adapt to, and mitigate the impacts on infrastructure and communities. The framework can also inform decision-making processes, such as the selection of optimal locations for infrastructure development and the allocation of resources for maintenance and repairs. The authors hope this study will stimulate further research into the development of more robust threat assessment frameworks.

Method

Threat assessment framework

The threat to the infrastructure due to warming permafrost is related to the extent of ground ice melted underneath. It is governed by the thermal regime in the ground and how it is affected by the warming climate. The ground thermal regime in the permafrost regions generally involves an active layer, i.e., the top layer of soil above permafrost that thaws and freezes seasonally, ranging from a fraction of a meter to a few meters in depth. The active layer thickness (ALT) can be affected by changes in the surface energy budget due to climate change or man-made alterations of the ground surface, such as water ponding, embankment, or snow accumulation. In cases where the

increase in Active Layer Thickness (ΔALT) extends to the permafrost boundary, it initiates thawing since the affected zone is no longer subject to sub-freezing temperatures. The thawing threat, i.e., the response of the frozen ground to changes in ground temperature, however, depends on soil type and the abundance, depth, and type of ground ice in the affected zone. Therefore, the changes in the ground thermal regime and the ground ice content are two key elements for threat assessment frameworks in regard to permafrost thaw.

The framework developed in this study (Fig. 7) uses an AI-based scheme to predict ground surface temperature by 2100, which is an indicator and a major driver affecting the ground thermal regime. It should be noted that the direct inclusion of ΔALT in the thaw index, while theoretically feasible, is often associated with greater uncertainties[56]. Therefore, and due to the scale of this study, mean annual ground surface temperature (MAGST) is used to represent the changes in the ground thermal regime. In regard to thaw susceptibility, the framework incorporates indices for the present abundance of various types of ground ice. The permafrost thaw threat index (I_t) is defined as:

$$I_t = f(MAGST) \cdot \left(\beta_s I_s + \beta_w I_w + \beta_r I_r\right) \quad (1)$$

where f is the thaw criteria function, the subscriptions w, r, and s stand for segregated, wedge, and relict ground ice, respectively, and β and I are weight factors and ground ice abundance indices, respectively. The thaw criteria function represents the impact of MAGST on the ground thermal regime and how changes in MAGST may result in thawing. At its simplest form, 0 °C is often defined as the border between frozen and unfrozen states, i.e., the function f is defined as a step function changing values from 0 to 1 at 0 °C. However, permafrost can exist where MAGST is above 0 °C due to differences in thermal conductivity of the active layer when frozen or thawed, which is known as the thermal offset[57,58]. Therefore, a non-linear thaw criterion is defined as:

$$f(MAGST) = \frac{1}{1 + e^{-MAGST}} \quad (2)$$

Ground temperature prediction scheme

The ground thermal regime is governed by the surface energy budget, i.e., the fluxes and processes that balance the energy between the ground and atmosphere. Several elements of the surface energy budget, for instance, solar radiation, wind, snow cover, and vegetation, are known to affect ground surface temperature. Therefore, it can be regarded as a supervised machine learning problem in which the ground surface temperature is the dependent variable, and conditions above the ground surface, such as ambient temperature, solar radiation, and snow depth, are independent variables.

The ground temperature forecasting scheme uses LSTM at its core. Models are individually trained over a geospatial grid using historical sequences of the dependent and independent climate variables from ERA5-Land reanalysis. In this study, the models were trained by ERA5-Land over a 0.1° x 0.1° spatial grid for each study site. The ambient temperature, shortwave and long-wave downward radiation, north-south and east-west wind speed, and snow depth were chosen as independent variables. For each node on the grid, the dataset contained daily values between 1950 and 2022, comprising more than 26,000 entries per node. The dataset was split into training and test sets in a 75%-25% ratio. A k-fold analysis was conducted in advance to monitor the model's performance with respect to unseen data. Once the models were trained, the independent variables from a regional

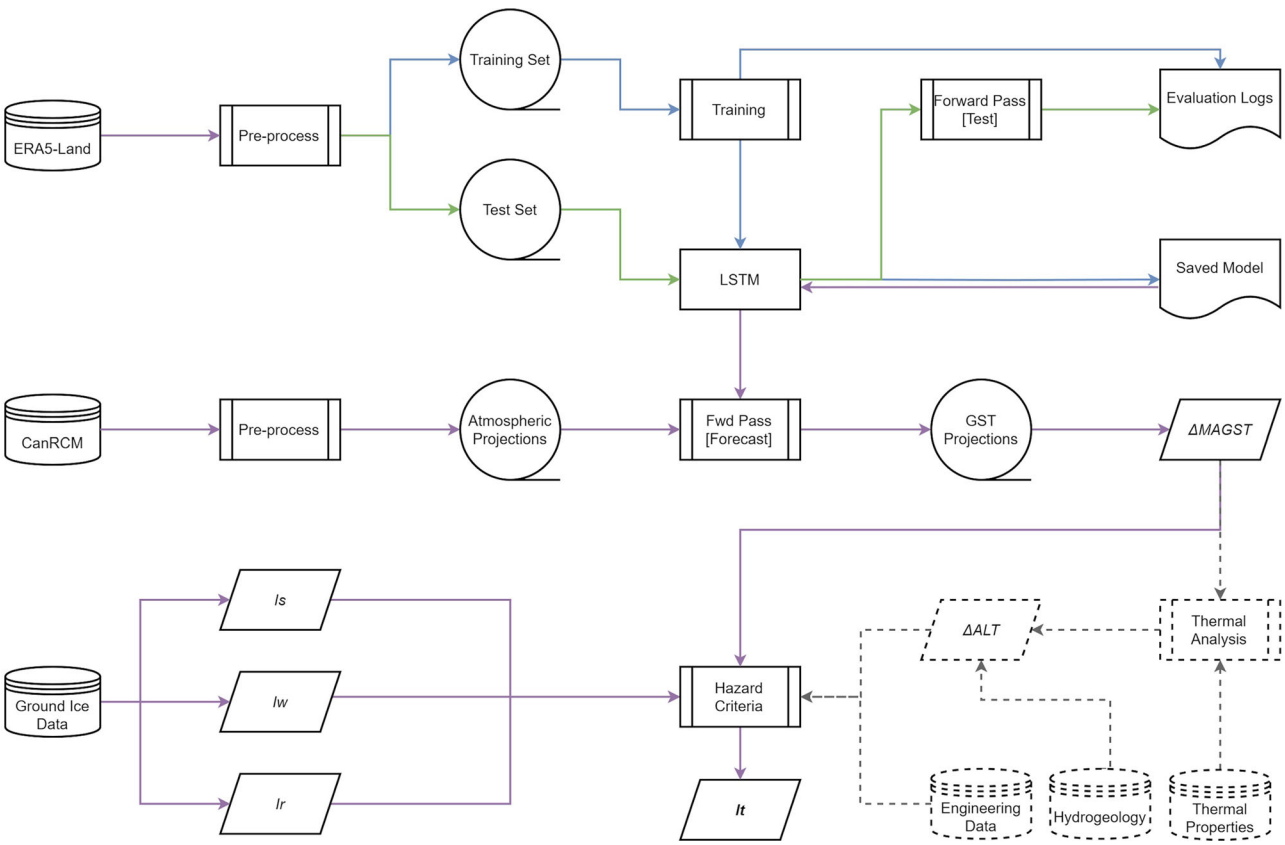

Fig. 7 | Schematics of the permafrost thaw threat assessment framework. The machine learning models are trained by multi-feature labeled data from ERA5-Land to predict ground surface temperature using CanRCM projections. The predicted ground surface temperatures and ground ice distributions are then used to calculate the thaw index, representing the permafrost thaw threat. Additional data, such as local subsurface properties and active layer depth, if available, can be integrated into the model to enhance accuracy at the local scale.

Table 3 | Training/test set and LSTM parameters used to train models at each study area

Test set ratio	Epochs	Batch Size	Input units	Sequence length	Layers	Hidden units
25%	50	100	6	7	1	50

Optimum model parameters were chosen based on sensitivity analyses using a similar model configuration[33].

Table 4 | Quantization of ground ice indices for segregated, wedge, and relic ice based on the presence of excess ground ice in the top 5 meters of permafrost from Ground Ice Map of Canada[20]

	None		Negligible		Low		Medium		High	
	%	$I_{s,w,r}$	%	$I_{s,w,r}$	%	$I_{s,w,r}$	%	$I_{s,w,r}$	%	$I_{s,w,r}$
Segregated ice	0	0	> 0 – 2	0.25	> 2 – 5	0.5	> 5 – 10	0.75	> 10	1
Wedge ice	0	0	> 0 – 2	0.25	> 2 – 5	0.5	> 5 – 10	0.75	> 10	1
Relict ice	0	0	> 0 – 2	0.25	> 2 – 5	0.5	> 5 – 10	0.75	> 10	1

climate model, in this case, daily projections of CanRCM, were fed to the models to predict daily ground surface temperatures over the grid. The MAGST is then calculated for RCP 4.5 and RCP 8.5, representing moderate and extreme climate change scenarios.

LSTM theory. LSTMs, as recurrent neural networks in general, are chains of repeating units. Each unit consists of a cell, which remembers values over time intervals, and gates that regulate the flow of information into and out of the cell. A classic LSTM cell has three cells: forget gate, an update (input) gate, and an output gate. The forget gate decides what information has to be removed from the cell state, i.e., forgotten from the memory. The input gate decides whether the cell state has to be updated, and the output gate controls the information passed to the next hidden state. During the forward pass in a classic LSTM, the forget gate first inspects the input data, the output of the previous cell and decides whether the information has to be kept or ignored:

$$f_t = \sigma\left(W_f \cdot \left[h_{t-1}, x_t\right] + b_f\right) \tag{3}$$

where f_t is the forget gate activation vector, $\sigma()$ is the sigmoid function, x_t is the input vector, h_{t-1} is the hidden state vector of the previous cell, and W_f and b_f are the weight matrices and bias vector of the forget layer, respectively, which are learnt during training. The update gate decides which information needs to be added to the cell state:

$$i_t = \sigma\left(W_i \cdot \left[h_{t-1}, x_t\right] + b_i\right) \tag{4}$$

in which i_t is the input (update) gate activation vector, and W_i and b_i are weight matrices and the bias vector of the update gate, respectively. A cell input candidate vector is then created as:

$$\tilde{c}_t = \tanh\left(W_c \cdot \left[h_{t-1}, x_t\right] + b_c\right) \tag{5}$$

where $\hat{c}_t$ is the vector of new candidate values, *tanh*() is the hyperbolic tangent function, and W_c and b_c are the weight matrices and bias vector, respectively. Having the forget and update activation vectors, f_t and i_t, the updated candidates c_t and the previous cell's state c_{t-1}, the current cell state c_t is updated as:

$$c_t = f_t * c_{t-1} + i_t * \tilde{c}_t \tag{6}$$

Finally, the cell output h_t is calculated from the cell state c_t and the activation vector of the output gate o_t, as follows:

$$o_t = \sigma\left(W_o\left[h_{t-1}, x_t\right] + b_o\right) \tag{7}$$

$$h_t = o_t * \tanh\left(c_t\right) \tag{8}$$

where W_o and b_o are the weight matrices and bias vectors of the output layer, respectively, which are learned during the training.

Table 3 presents the parameters used for model training. The parameters, such as the sequence length and the number of hidden units, have been selected based on sensitivity analyses in a previous study[33].

Ground ice indices

The ground ice indices I_s, I_w, I_r are based on the Ground Ice Map of Canada (GIMC)[20]. The GIMC uses a paleogeographic approach to model and present the abundance of ground ice in the top 5 m of permafrost across Canada. It classifies ground ice into three categories as:

- Relic ice: Bodies of ice that are preserved under overburden, either in the form of buried glacier ice or intrasedimental ice. In Canada, relict ice is most abundant in continuous permafrost in the western Arctic, which has remained preserved in glaciogenic sediments.
- Segregated ice: Ice layers that are formed by migration of pore water toward the freezing front, which are widely distributed in fine-grained deposits of glacial lakes and marine sediments.
- Wedge ice: Ice that is formed by infilling water in thermal cracks in the ground and grown over time by repeated cracking, infilling, and freezing. It is mostly present in the western Arctic.

For each type of ground ice, GIMC qualitatively reports the abundance as high, medium, low, negligible and none. Here, in order to develop the ground ice indices, the GIMC's rasters for each type of ground ice type were sampled over the ERA grid in the GIS software. The sampled data was then transferred into the normalized quantitative form to obtain I_s, I_w, I_r, each ranging from 0 (no ground ice) to 1 (high abundance), as shown in Table 4. It should be noted that the differences in thawing effects for different ground ice types were not in the scope of work of this study. Therefore, the weight factors were assumed as β_s, β_w, $\beta_r = 0.33$, resulting in the thaw index I_t ranging from 0 to 1.

Data availability

The ERA5-Land data products are available on the European Center for Medium-Range Weather Forecasts's (ECMWF) Climate Data Store (CDS) under the Creative Commons Attribution 4.0 International (CC BY 4.0) license at https://cds.climate.copernicus.eu/cdsapp#!/dataset/10.24381/cds.e2161bac[59]. The CanRCM projections are accessible at the Canadian Center for Climate Modeling and Analysis data store under the owner's unrestricted license at https://climate-modeling.canada.ca/climatemodeldata/canrcm/CanRCM4[60]. The ground ice map of Canada is available on Natural Resources Canada's GEOSCAN database under the Government of Canada's Open Government License at https://ostrnrcan-dostrncan.canada.ca/entities/publication/8824ac4e-77b9-4cc8-86b5-4aea4ba7e912[61]. The authors have publicly released model outputs and evaluation results (Supplementary Data 1–4) at https://zenodo.org/records/10506941and the

source data for graphs at https://zenodo.org/records/10507395, both under the Creative Commons Attribution 4.0 International (CC BY 4.0) license[62,63].

Code availability

The authors have publicly released the ground surface temperature forecasting framework source code under the GNU General Public License 3.0 (GPLv3) at https://github.com/siglab-team/janus[64].

Received: 22 June 2023; Accepted: 12 March 2024;
Published online: 30 March 2024

References

1. Glomsrød, S., Duhaime, G. & Aslaksen, I. *The Economy of the North-ECONOR 2020* (Arctic Council, 2021).
2. Glomsrød, S. & Aslaksen, I. *The Economy of the North-ECONOR 2006* (Statistics Norway, 2006).
3. Heleniak, T. The future of the arctic populations. *Polar Geography* **44**, 136–152 (2021).
4. Dawson, J., Pizzolato, L., Howell, S. E., Copland, L. & Johnston, M. E. Temporal and spatial patterns of ship traffic in the canadian arctic from 1990 to 2015. *Arctic* **71**, 15–26 (2018).
5. Mudryk, L. R. et al. Impact of 1, 2 and 4 c of global warming on ship navigation in the canadian arctic. *Nat. Clim. Change* **11**, 673–679 (2021).
6. Fedorov, A. N. et al. Permafrost-landscape map of the republic of sakha (yakutia) on a scale 1:1,500,000. *Geosciences* **8**, 465 (2018).
7. Gruber, S. Derivation and analysis of a high-resolution estimate of global permafrost zonation. *The Cryosphere* **6**, 221–233 (2012).
8. Obu, J. How much of the earth's surface is underlain by permafrost? *J. Geophys. Res.: Earth Surface* **126**, e2021JF006123 (2021).
9. Liu, H., Maghoul, P. & Shalaby, A. Seismic physics-based characterization of permafrost sites using surface waves. *Cryosphere* **16**, 1157–1180 (2022).
10. Ramage, J. et al. Population living on permafrost in the arctic. *Popul. Environ.* **43**, 22–38 (2021).
11. Hjort, J. et al. Degrading permafrost puts arctic infrastructure at risk by mid-century. *Nat. Commun.* **9**, 1–9 (2018).
12. IPCC. *Climate Change 2021: The Physical Science Basis. Contribution of Working Group I to the Sixth Assessment Report of the Intergovernmental Panel on Climate Change*, vol. In Press (Cambridge University Press, Cambridge, United Kingdom and New York, NY, USA, 2021).
13. Biskaborn, B. K. et al. Permafrost is warming at a global scale. *Nat. Commun.* **10**, 1–11 (2019).
14. Chadburn, S. et al. An observation-based constraint on permafrost loss as a function of global warming. *Nat. Clim. Change* **7**, 340–344 (2017).
15. Amini, D., Maghoul, P., Holländer, H. & Bilodeau, J.-P. A critical state-based thermo-elasto-viscoplastic constitutive model for thermal creep deformation of frozen soils. *Acta Geotech*. https://doi.org/10.1007/s11440-023-02058-1.
16. Andersland, O. B. & Ladanyi, B.*Frozen ground engineering* (Springer New York, NY, 2013).
17. Kokelj, S. V. & Jorgenson, M. T. Advances in thermokarst research. *Permafrost Periglacial Processes* **24**, 108–119 (2013).
18. Luo, J., Niu, F., Lin, Z., Liu, M. & Yin, G. Thermokarst lake changes between 1969 and 2010 in the beilu river basin, qinghai-tibet plateau, china. *Sci. Bull.* **60**, 556–564 (2015).
19. Doré, G., Niu, F. & Brooks, H. Adaptation methods for transportation infrastructure built on degrading permafrost. *Permafrost Periglacial Processes* **27**, 352–364 (2016).
20. O'Neill, H. B., Wolfe, S. A. & Duchesne, C. New ground ice maps for canada using a paleogeographic modelling approach. *Cryosphere* **13**, 753–773 (2019).
21. Karjalainen, O. et al. Circumpolar permafrost maps and geohazard indices for near-future infrastructure risk assessments. *Sci. Data* **6**, 1–16 (2019).
22. Westermann, S., Lüers, J., Langer, M., Piel, K. & Boike, J. The annual surface energy budget of a high-arctic permafrost site on svalbard, norway. *Cryosphere* **3**, 245–263 (2009).
23. Kong, X., Doré, G. & Calmels, F. Thermal modeling of heat balance through embankments in permafrost regions. *Cold Regions Sci. Technol.* **158**, 117–127 (2019).
24. Riseborough, D., Shiklomanov, N., Etzelmüller, B., Gruber, S. & Marchenko, S. Recent advances in permafrost modelling. *Permafrost Periglacial Processes* **19**, 137–156 (2008).
25. Tabari, H., Hosseinzadeh Talaee, P. & Willems, P. Short-term forecasting of soil temperature using artificial neural network. *Meteorol. Appl.* **22**, 576–585 (2015).
26. Feng, Y., Cui, N., Hao, W., Gao, L. & Gong, D. Estimation of soil temperature from meteorological data using different machine learning models. *Geoderma* **338**, 67–77 (2019).
27. Zeynoddin, M. et al. A reliable linear stochastic daily soil temperature forecast model. *Soil Tillage Res.* **189**, 73–87 (2019).
28. Hochreiter, S. & Schmidhuber, J. Long short-term memory. *Neural Comput.* **9**, 1735–1780 (1997).
29. Sherstinsky, A. Fundamentals of recurrent neural network (rnn) and long short-term memory (lstm) network. *Phys. D: Nonlinear Phenomena* **404**, 132306 (2020).
30. Li, Q. et al. An attention-aware lstm model for soil moisture and soil temperature prediction. *Geoderma* **409**, 115651 (2022).
31. Yang, Y. et al. A cfcc-lstm model for sea surface temperature prediction. *IEEE Geosci. Remote Sens. Lett.* **15**, 207–211 (2018).
32. Gao, B., Huang, X., Shi, J., Tai, Y. & Xiao, R. Predicting day-ahead solar irradiance through gated recurrent unit using weather forecasting data. *J. Renewable Sustainable Energy* **11**, 043705 (2019).
33. Fatolahzadeh Gheysari, A., Maghoul, P., Ashraf, A., Shalaby, A. & Roy, K. Ai-powered ground surface temperature forecasting for cold regions geotechnical applications (2022). Paper presented at the 75th Canadian Geotechnical Conference (GeoCalgary2022), Calgary, Alberta, Canada, 2–5 October 2022.
34. Biskaborn, B. K. et al. The new database of the global terrestrial network for permafrost (gtn-p). *Earth Syst. Sci. Data* **7**, 245–259 (2015).
35. Bengtsson, L. et al. The need for a dynamical climate reanalysis. *Bull. Am. Meteorol. Soc.* **88**, 495–501 (2007).
36. Laloyaux, P., Balmaseda, M., Dee, D., Mogensen, K. & Janssen, P. A coupled data assimilation system for climate reanalysis. *Quart. J. R. Meteorol. Soc.* **142**, 65–78 (2016).
37. Gelaro, R. et al. The modern-era retrospective analysis for research and applications, version 2 (merra-2). *J. Clim.* **30**, 5419–5454 (2017).
38. Hersbach, H. et al. The era5 global reanalysis. *Quart. J. R. Meteorol. Soc.* **146**, 1999–2049 (2020).
39. Graham, R. M., Hudson, S. R. & Maturilli, M. Improved performance of era5 in arctic gateway relative to four global atmospheric reanalyses. *Geophys. Res. Lett.* **46**, 6138–6147 (2019).
40. Taszarek, M. et al. Comparison of convective parameters derived from era5 and merra2 with rawinsonde data over europe and north america. *J. Clim.* **34**, 3211–3237 (2021).
41. Muñoz Sabater, J. et al. Era5-land: a state-of-the-art global reanalysis dataset for land applications. *Earth Syst. Sci. Data* **13**, 4349–4383 (2021).
42. Cao, B., Gruber, S., Zheng, D. & Li, X. The era5-land soil temperature bias in permafrost regions. *Cryosphere* **14**, 2581–2595 (2020).
43. Xie, W. et al. The evaluation of imerg and era5-land daily precipitation over china with considering the influence of gauge data bias. *Sci. Rep.* **12**, 8085 (2022).
44. Fatolahzadeh Gheysari, A., Maghoul, P., Ojo, E. R. & Shalaby, A. Reliability of era5 and era5-land reanalysis data in the canadian prairies. *Theor. Appl. Climatol.* **155**, 3087–3098 (2024).

45. Han, L. et al. A machine learning nowcasting method based on real-time reanalysis data. *J. Geophys. Res.: Atmos.* **122**, 4038–4051 (2017).
46. Kleynhans, T., Montanaro, M., Gerace, A. & Kanan, C. Predicting top-of-atmosphere thermal radiance using merra-2 atmospheric data with deep learning. *Remote Sens.* **9**, 1133 (2017).
47. He, Y., Chen, C., Li, B. & Zhang, Z. Prediction of near-surface air temperature in glacier regions using era5 data and the random forest regression method. *Rem. Sens. Appl. Soc. Environ.* **28**, 100824 (2022).
48. Addison, P. E., Oommen, T. & Lautala, P. A review of past geotechnical performance of the hudson bay rail embankment and its comparison to the current condition. In *Proceedings of the 2015 Joint Rail Conference*, vol. 2015 Joint Rail Conference of *ASME/IEEE Joint Rail Conference* (2015).
49. Hayley, D. Maintenance of a railway grade over permafrost in canada. In *Proceedings of the 5th International Conference on Permafrost*, 43–48 (1988).
50. Oommen, T., Lautala, P. & Addison, P. Rail embankment stabilization needs on the hudson bay railway. Tech. Rep., Michigan Technological University https://rosap.ntl.bts.gov/view/dot/32054 (2017).
51. Lantz, T. C. & Kokelj, S. V. Increasing rates of retrogressive thaw slump activity in the mackenzie delta region, n.w.t., canada. *Geophys. Res. Lett.* **35**, L06502 (2008).
52. Cohen, J. et al. Recent arctic amplification and extreme mid-latitude weather. *Nat. Geosci.* **7**, 627–637 (2014).
53. Hengl, T. et al. Soilgrids1km — global soil information based on automated mapping. *PLOS ONE* **9**, 1–17 (2014).
54. Peppin, S. S. L. & Style, R. W. The physics of frost heave and ice-lens growth. *Vadose Zone J.* **12**, 1–12 (2013).
55. Kokelj, S. V., Lantz, T. C., Tunnicliffe, J., Segal, R. & Lacelle, D. Climate-driven thaw of permafrost preserved glacial landscapes, northwestern canada. *Geology* **45**, 371–374 (2017).
56. Aalto, J., Karjalainen, O., Hjort, J. & Luoto, M. Statistical forecasting of current and future circum-arctic ground temperatures and active layer thickness. *Geophys. Res. Lett.* **45**, 4889–4898 (2018).
57. Throop, J., Lewkowicz, A. G. & Smith, S. L. Climate and ground temperature relations at sites across the continuous and discontinuous permafrost zones, northern canada. *Can. J. Earth Sci.* **49**, 865–876 (2012).
58. Romanovsky, V. E. & Osterkamp, T. E. Interannual variations of the thermal regime of the active layer and near-surface permafrost in northern alaska. *Permafrost Periglacial Processes* **6**, 313–335 (1995).
59. Muñoz-Sabater, J. Era5-land hourly data from 1981 to present (2019). [Accessed 2024-01-03].
60. Canadian Centre for Climate Modelling and Analysis. Canrcm4 model output https://climate-modelling.canada.ca/climatemodeldata/canrcm/CanRCM4 (2023). [Accessed 2024-01-03].
61. O'Neill, H., Wolfe, S. & Duchesne, C. Ground ice map of canada (2022). [Accessed 2024-01-03].
62. Fatolahzadeh Gheysari, A. & Maghoul, P. A framework to assess permafrost thaw threat for land transportation infrastructure in northern canada [supplementary information] (2024).
63. Fatolahzadeh Gheysari, A. & Maghoul, P. A framework to assess permafrost thaw threat for land transportation infrastructure in northern canada [figures source data] (2024).
64. Fatolahzadeh Gheysari, A. Janus: a machine learning framework for dependent climate variables forecasting (2024).

Acknowledgements

We acknowledge the financial support of the New Frontiers in Research Fund—Exploration Grant [NFRF-390 2018-00966] and the Mitacs E-Accelerate program [IT20113].

Author contributions

A.F.G.: conceptualization, model development, data curation, formal analysis, investigation, writing—original draft, visualization. P.M.: conceptualization, model development, investigation, writing - review and editing, supervision, project administration, funding acquisition.

Competing interests

The authors declare no competing interests.

Additional information

Supplementary information The online version contains supplementary material available at https://doi.org/10.1038/s43247-024-01317-7.

Correspondence and requests for materials should be addressed to Pooneh Maghoul.

Peer review information *Communications Earth & Environment* thanks Heather Brooks and the other, anonymous, reviewer(s) for their contribution to the peer review of this work. Primary Handling Editors: Martina Grecequet, Joe Aslin. A peer review file is available.